JGP Journal of General Physiology

RESEARCH ARTICLE

Ligand binding and activation properties of the purified bacterial cyclic nucleotide–gated channel SthK

Philipp A.M. Schmidpeter[1*], Xiaolong Gao[1*], Vikrant Uphadyay[1], Jan Rheinberger[1], and Crina M. Nimigean[1,2,3]

Cyclic nucleotide–modulated ion channels play several essential physiological roles. They are involved in signal transduction in photoreceptors and olfactory sensory neurons as well as pacemaking activity in the heart and brain. Investigations of the molecular mechanism of their actions, including structural and electrophysiological characterization, are restricted by the availability of stable, purified protein obtained from accessible systems. Here, we establish that SthK, a cyclic nucleotide–gated (CNG) channel from *Spirochaeta thermophila*, is an excellent model for investigating the gating of eukaryotic CNG channels at the molecular level. The channel has high sequence similarity with its eukaryotic counterparts and was previously reported to be activated by cyclic nucleotides in patch-clamp experiments with *Xenopus laevis* oocytes. We optimized protein expression and purification to obtain large quantities of pure, homogeneous, and active recombinant SthK protein from *Escherichia coli*. A negative-stain electron microscopy (EM) single-particle analysis indicated that this channel is a promising candidate for structural studies with cryo-EM. Using radioactivity and fluorescence flux assays, as well as single-channel recordings in lipid bilayers, we show that the protein is partially activated by micromolar concentrations of cyclic adenosine monophosphate (cAMP) and that channel activity is increased by depolarization. Unlike previous studies, we find that cyclic guanosine monophosphate (cGMP) is also able to activate SthK, but with much lower efficiency than cAMP. The distinct sensitivities to different ligands resemble eukaryotic CNG and hyperpolarization-activated and cyclic nucleotide–modulated channels. Using a fluorescence binding assay, we show that cGMP and cAMP bind to SthK with similar apparent affinities, suggesting that the large difference in channel activation by cAMP or cGMP is caused by the efficacy with which each ligand promotes the conformational changes toward the open state. We conclude that the functional characteristics of SthK reported here will permit future studies to analyze ligand gating and discrimination in CNG channels.

Introduction

Cyclic nucleotide–modulated ion channels link the intracellular levels of second messengers, such as cAMP and cGMP, to cellular electrical responses. These channels include hyperpolarization-activated and cyclic nucleotide–modulated (HCN) and CNG channels, which are members of the S4 superfamily of voltage-dependent channels (Yellen, 2002; Yu and Catterall, 2003). Structurally, these channels are tetramers (Fig. 1 A), and each subunit can be further divided into a transmembrane domain and a cytoplasmic cyclic nucleotide–binding domain (CNBD; Craven and Zagotta, 2006). The transmembrane domain consists of six membrane-spanning helices (S1–S6) where S1–S4 form a voltage-sensor domain and S5–S6, the pore domain that is linked to the CNBD via a helical C-linker (Fig. 1 A). Depending on the channel, the CNBD binds cAMP and/or cGMP with nano- to micromolar affinities, which leads to conformational changes that gate these channels. Although structurally similar, CNG and HCN channels show considerable functional differences (Kaupp and Seifert, 2002; Robinson and Siegelbaum, 2003; Craven and Zagotta, 2006; James and Zagotta, 2018). CNG channels require cyclic nucleotide binding to open the channel (Karpen et al., 1988; Kaupp et al., 1989), whereas HCN channels are activated by membrane hyperpolarization, and their activity is only modulated by cyclic nucleotide binding (Ludwig et al., 1998; Craven and Zagotta, 2006). The sea urchin HCN channel is a special case because it is both hyperpolarization dependent and cyclic nucleotide activated (Gauss et al., 1998). CNG channels are nonselective cation channels, which can conduct monovalent and divalent cations to generate primary electric signals in photoreceptors

[1]Department of Anesthesiology, Weill Cornell Medicine, New York, NY; [2]Department of Biochemistry, Weill Cornell Medicine, New York, NY; [3]Department of Physiology and Biophysics, Weill Cornell Medicine, New York, NY.

*P.A.M. Schmidpeter and X. Gao contributed equally to this paper; Correspondence to Crina M. Nimigean: crn2002@med.cornell.edu.

and olfactory sensory neurons. In contrast, HCN channels are weakly selective for K^+ over Na^+ and are expressed mostly in the heart and brain, where they are important for pacemaking activity and autonomous rhythmicity (Biel et al., 2009).

Structural information on the isolated CNBDs from prokaryotic and eukaryotic channels is available from x-ray crystallography and nuclear magnetic resonance spectroscopy (Zagotta et al., 2003; Flynn et al., 2007; Altieri et al., 2008; Xu et al., 2010; Lolicato et al., 2011; Kesters et al., 2015). Full-length prokaryotic HCN/CNG channels have been studied by cryoelectron microscopy (cryo-EM; MloK1 and LliK channels; Chiu et al., 2007; Kowal et al., 2014, 2018; James et al., 2017), and recently single-particle cryo-EM was used to solve the structures of human HCN1 (Lee and MacKinnon, 2017), as well as TAX-4 (Li et al., 2017), a CNG channel from *Caenorhabditis elegans*. However, MloK1 and LliK cannot be used for detailed functional studies because they do not show single-channel currents in planar lipid bilayers. The eukaryotic channels are difficult to express, purify, and reconstitute in the quantities necessary for structural and functional studies. Furthermore, HCN1 is only marginally modulated by cyclic nucleotides, and because it has very small single-channel conductance, it is not conducive to single-channel analysis (DiFrancesco, 1986; Accili et al., 2002; Lee and MacKinnon, 2017). Because of limited functional data available (Komatsu et al., 1999; Paoletti et al., 1999; Li et al., 2017), the newly solved TAX-4 structure only allows for coarse structure–function correlations. All these drawbacks highlight the need to establish a cost-efficient, biochemical, structural, and functional model system suitable for an array of biochemical and biophysical assays to elaborate the functional molecular mechanism of cyclic nucleotide–modulated channels.

Recently, several putative cyclic nucleotide–modulated, prokaryotic K^+ channels with high sequence similarities (24–32%) to their eukaryotic counterparts were identified (Brams et al., 2014). They all share the same domain architecture: a voltage-sensor domain (S1–S4), a pore domain (S5–S6), and a cytosolic C-linker/CNBD domain (Fig. 1 A and Fig. S1). One of those channels, SthK (from *Spirochaeta thermophila*), was previously reported to express in *Escherichia coli*, albeit in low quantities, as well as in *Xenopus laevis* oocytes (Brams et al., 2014). Patch-clamp experiments of SthK expressed in oocytes demonstrated cAMP-dependent activity, selectivity for K^+ over Na^+, and inhibition by cGMP. In this work, we optimized the gene construct and the conditions for expression and purification, and we were able to obtain milligram quantities of pure, homogeneous, and active SthK channel protein from *E. coli*. The large quantities of purified protein available allowed us to perform multiple functional and structural assays that are quasi-inaccessible for eukaryotic channels, and we established the SthK channel as a bona fide model for its eukaryotic homologues because it shares features with both HCN and CNG channels. Furthermore, by combining binding and activity assays, we determined that cGMP is not an antagonist as previously reported (Brams et al., 2014); rather, it is an extremely poor, partial agonist for SthK, and its low efficiency compared with cAMP in activating the channel is not caused by low intrinsic binding affinity. The ability to determine the function and regulation of this channel with different assays under

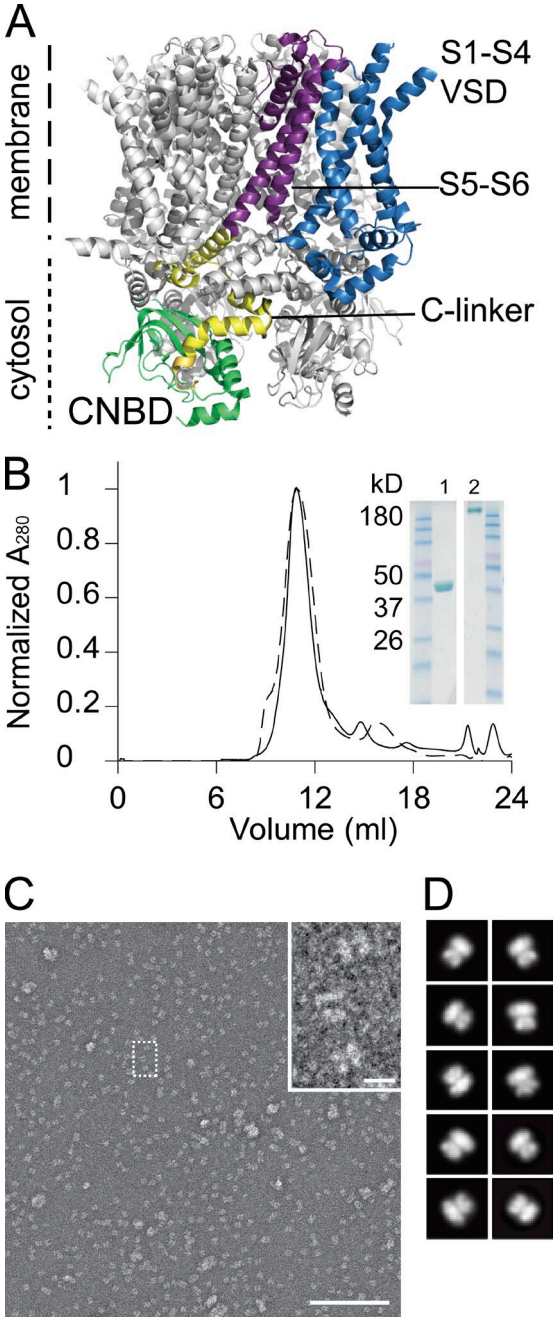

Figure 1. **SthK topology and purification details. (A)** Cartoon representation of the HCN1 channel structure (Lee and MacKinnon, 2017; Protein Data Bank accession no. 5U6O) as a model to highlight the domain architecture of the homologous SthK channel. One subunit of the channel is shown with the S1–S4 in blue, S5–S6 in purple, the C-linker in yellow, the CNBD in green, and the remaining three subunits in gray. The figure was prepared using PyMol (http://www.pymol.org). **(B)** Elution profile from size-exclusion chromatography (Superdex 200 10/300 GL) for SthK in the presence (solid line) and absence (dashed line) of cAMP; the inset shows an SDS-PAGE analysis of purified SthK (lane 1) and the results of cross-linking with 0.12% glutaraldehyde, confirming tetrameric assembly of SthK (lane 2). BenchMark Prestained Protein Ladder (Life Technologies) was used to estimate the molecular weight. **(C)** A representative negative-stain EM micrograph (bar, 141 nm) is shown to illustrate the quality of the final protein sample. A few representative particles used for 2-D classification are highlighted (small box) and enlarged in the inset (top, right; bar, 10 nm). **(D)** The resulting 2-D classes (box size, 248 Å) from negative-stain images are shown.

defined conditions, the amenability of this channel to structural analyses, and the similarity between SthK and eukaryotic channels make this channel an excellent working model for understanding gating and dynamics of cyclic nucleotide–modulated channels in molecular detail.

Materials and methods

SthK expression and protein purification

The gene for SthK (UniProt accession no. G0GA88) was cloned into the vector pCGFP-BC (Kawate and Gouaux, 2006) between the restriction sites for HindIII and XhoI, which adds 19 residues from the multiple cloning sites to the N terminus of the channel. These residues do not affect the channel function but help with the expression and stability of the final, purified protein. Small-scale expression and detergent screens were performed with fluorescence-detection size-exclusion chromatography (Kawate and Gouaux, 2006), in which the supernatant from a crude extract was applied to a Superdex 200 Increase 5/150 column (GE Healthcare Life Sciences) in 20 mM HEPES, 100 mM KCl, 200 µM cAMP, pH 7.4, and 2× critical micellar concentration of different detergents. After the initial screening, the GFP gene and four histidine residues from the octa-histidine tag were deleted from the vector by Quikchange (Agilent Technologies) mutagenesis, and protein expression was performed in *E. coli* C41 (DE3; Lucigen). Cells were grown in Luria-Bertani broth at 37°C to an OD_{600nm} of 0.4, transferred to 20°C, and further grown to an OD_{600nm} of 0.8, when protein expression was induced with 0.5 mM isopropyl β-D-1-thiogalactopyranoside for 12 h. The cells were harvested by centrifugation at 4,000 *g* for 10 min at 4°C. Subsequent steps were all performed at 4°C, except for the final size-exclusion chromatography, which was performed at room temperature. Cells from 4-liter cultures were resuspended in 50 ml lysis buffer (50 mM Tris, pH 7.8, at room temperature; 100 mM KCl; and 200 µM cAMP) supplemented with PMSF (85 µg/ml), leupeptin/pepstatin (0.95/1.4 µg/ml), DNaseI (1 mg; MilliporeSigma), lysozyme (1 mg; MilliporeSigma), and cOmplete ULTRA mini protease inhibitor (Roche). Cells were lysed by sonication with a Sonic Dismembrator 500 (Thermo Fisher Scientific). Membrane proteins were extracted and solubilized with 30 mM *n*-dodecyl-β-D-maltopyranoside (DDM; Anatrace) for 1.5 h at 4°C. Cell debris was pelleted by centrifugation at 36,000 *g* for 45 min. The supernatant was filtered through a 0.22-µm filter and loaded onto a 5-ml HiTrap chelating HP Co^{2+} column (GE Healthcare Life Sciences), preequilibrated with purification buffer (20 mM HEPES, pH 7.8, 100 mM KCl, 200 µM cAMP, and 0.5 mM DDM). Proteins not specifically bound were removed by washing the column with 15-column volumes of purification buffer containing 30 mM imidazole before SthK was eluted with purification buffer containing 300 mM imidazole. The eluate was concentrated to 10 mg/ml with an Amicon ultra concentrator (MilliporeSigma) with a 100-kD cutoff before loading the sample on a Superdex 200 10/300 GL column (GE Healthcare Life Sciences) preequilibrated in purification buffer, unless otherwise noted. The peak fraction containing purified SthK was collected for further structural and functional studies. The final protein concentration was determined from the absorbance at 280 nm using a molar extinction coefficient of 55,900 M^{-1} cm^{-1}. The ratio A_{260}/A_{280} was used as a criterion to estimate the cAMP content in the sample.

Fluorescence binding assay

To measure the binding constants of cAMP and cGMP for SthK, the cAMP used during purification needed to be removed. Because the apo-SthK in detergent is prone to aggregation, we exchanged DDM for amphipol (A8-35; Anatrace) for equilibrium titrations. After concentrating the eluted protein from the immobilized metal ion affinity chromatography column, amphipol A8-35 hydrated in double-distilled H_2O was added (1:3 wt/wt, protein/amphipol) and the protein–amphipol mixture was incubated at 4°C for 1 h under gentle agitation. Subsequently, the sample was applied to a detergent-removal column (Thermo Fisher Scientific) and further purified by size-exclusion chromatography (Superdex 200 10/300 GL) in 20 mM HEPES and 100 mM KCl, pH 7.4 (without detergent and cAMP). The absorbance ratio A_{260}/A_{280} of the final sample was typically 0.52. For comparison, the same absorbance ratio for a cAMP-containing sample was 0.72.

Fluorescence titrations in equilibrium were performed in 20 mM HEPES and 100 mM KCl, pH 7.4, at room temperature with a fluorescence spectrometer (Photon Technology International) and the fluorescent cAMP/cGMP analogues 8-NBD-cAMP/cGMP (fcAMP/fcGMP; Biolog). The fluorescence of 0.1 µM fcAMP/fcGMP was measured at 536 nm after excitation at 463 nm (5 nm bandwidth each) upon titration with increasing concentrations of SthK in A8-35, with the concentration of fcAMP/fcGMP kept constant. According to a stoichiometric complex formation (Eq. 1 and 2) in equilibrium, in which each monomer of SthK can bind one molecule of ligand, and considering mass conservation, the fluorescence was correlated to the extent of the complex formation (Eq. 3), and the data were fitted according to (Wilkinson, 2004) to obtain the apparent K_d value for the interaction between 8-NBD-cAMP/cGMP and SthK:

$$\mathrm{SthK} + \mathrm{cNMP} \rightleftarrows \mathrm{SthK} \cdot \mathrm{cNMP} \tag{1}$$

$$K_d = \frac{[\mathrm{SthK}] \cdot [\mathrm{cNMP}]}{[\mathrm{SthK} \cdot \mathrm{cNMP}]} \tag{2}$$

$$F = F_{min} + \left(F_{max} - F_{min}\right) \cdot \frac{[\mathrm{SthK} \cdot \mathrm{cNMP}]}{[\mathrm{cNMP}]_0} \tag{3}$$

and

$$F\left(\left[\mathrm{SthK}\right]\right) = F_{min} + \left(F_{max} - F_{min}\right) \cdot \frac{\left([\mathrm{SthK}]_0 + [\mathrm{cNMP}]_0 + K_d\right) - \sqrt{\left(-[\mathrm{SthK}]_0 - [\mathrm{cNMP}]_0 - K_d\right)^2 - 4 \cdot [\mathrm{SthK}]_0 \cdot [\mathrm{cNMP}]_0}}{2 \cdot [\mathrm{cNMP}]_0} \tag{4}$$

where [SthK] and [cNMP] are the concentrations of the free, interacting partners; [SthK · cNMP] is the complex of both; F_{min} and F_{max} are the minimum and the maximum fluorescence, respectively; $[\mathrm{SthK}]_0$ and $[\mathrm{cNMP}]_0$ are the total concentrations of the interacting molecules in micromolars; and K_d is the dissociation constant in micromolars.

For competition experiments, 0.3 µM fcAMP, mixed with 0.3 µM SthK in A8-35, was titrated with increasing amounts of nonfluorescent cAMP or cGMP, keeping the concentrations of

fcAMP and SthK constant. Fluorescence was monitored at 536 nm after excitation at 463 nm (5-nm bandwidth each). Because the measured signal change in this case reflects the binding equilibria between the channel and two ligands (Eq. 5), the binding term is a more complex, cubic function (Wilkinson, 2004; Cukkemane et al., 2007; for derivation, see Wang, 1995). Data analysis was performed by solving the depressed cubic function for the real root (Eq. 6; Wang, 1995; Wilkinson, 2004; Cukkemane et al., 2007), giving the apparent affinities for both the fluorescent and the nonfluorescent ligands. It is important to point out that, in the simplified model (Eq. 5), SthK describes a single subunit in the tetramer:

$$\mathrm{SthK \cdot cNMP + fcAMP} \rightleftarrows \mathrm{SthK + fcAMP + cNMP} \rightleftarrows \mathrm{SthK \cdot fcAMP + cNMP} \quad (5)$$

and

$$F = F_{\min} + \left(F_{\max} - F_{\min}\right) \cdot \frac{2 \cdot \sqrt{\left(a^2 - 3b\right)} \cdot \cos\left(\frac{\theta}{3}\right) - a}{3 \cdot K_a + \left[2 \cdot \sqrt{\left(a^2 - 3b\right)} \cdot \cos\left(\frac{\theta}{3}\right) - a\right]} \quad (6)$$

with Eq. 7:

$$\theta = \arccos \cdot \frac{-2a^3 + 9ab - 27c}{2 \cdot \sqrt{(a^2 - 3b)^3}} \quad (7)$$

where $a = K_a + K_b + [A_t] + [B_t] - [P_t]$; $b = K_b \cdot ([A_t] - [P_t]) + K_a \cdot ([B_t] - [P_t]) + K_a \cdot K_b$; $c = -K_a \cdot K_b \cdot [P_t]$; F is the monitored fluorescence; F_{min} and F_{max} are the minimum and maximum fluorescence, respectively; $[A_t]$, $[B_t]$, and $[P_t]$ are the total concentrations of the fluorescent ligand, the nonfluorescent ligand, and the receptor concentration in micromolars, respectively; and K_a and K_b are the binding constants in micromolars of the fluorescent and nonfluorescent ligands, respectively.

Channel reconstitution and rubidium flux assays

Immediately after gel filtration, SthK was reconstituted into liposomes (Heginbotham et al., 1998). 1,2-Dioleoyl-*sn*-glycero-3-phosphocholine (DOPC), 1-palmitoyl-2-oleoyl-*sn*-glycero-3-phospho-(1′-*rac*-glycerol) (POPG), and 18:1 cardiolipin in chloroform (Avanti Polar Lipids) or 1-palmitoyl-2-oleoyl-*sn*-glycero-3-phosphoethanolamine (POPE) and POPG in chloroform were mixed at a ratio of 5:3:2 (wt/wt/wt) or 3:1 (wt/wt), respectively, and dried under nitrogen flow. Lipids were resolubilized with 34 mM CHAPS (3-((3-cholamidopropyl) dimethylammonio)-1-propanesulfonate) in reconstitution buffer (10 mM HEPES, 400 mM KCl, and 5 mM NMG [*N*-methylglucamine gluconate], pH 7.6) to a final lipid concentration of 10 mg/ml. After mixing with 30 µg SthK per milligram of solubilized lipids, detergent was removed by applying the sample (500 µl) to an 18-ml detergent-removal column (Sephadex G-50 fine beads, GE Healthcare Life Sciences). Proteoliposomes were aliquoted, flash frozen in liquid nitrogen, and stored at −80°C. Liposomes without SthK were prepared in parallel as a control for each flux experiment.

The $^{86}Rb^+$ flux assay was performed as described earlier (Nimigean, 2006). In brief, the extra-liposomal solution was exchanged by passing 100 µl of liposomes through 1.5 ml G50 spin columns (Sigma) equilibrated with sorbitol buffer (10 mM HEPES, 400 mM sorbitol, 4 mM NMG, pH 7.6, and 5 µM KCl) containing the same cAMP or cGMP concentrations as inside the liposomes. Radioactive uptake was initiated by adding sorbitol buffer containing $^{86}Rb^+$ (1 µCi/ml) to the liposomes. 100-µl samples were taken at the desired time points and passed through 1.5-ml Dowex cation exchange columns equilibrated with 400 mM sorbitol to remove the extraliposomal $^{86}Rb^+$. At the end of each experiment, 1 µg/ml valinomycin was added to the remaining liposomes to determine the maximum amount of $^{86}Rb^+$ uptake, to which all measurements from an individual experiment were normalized. Scintillation fluid was added to each sample, and the radioactivity was measured with a liquid scintillation counter. All experiments were performed in triplicates.

Stopped-flow fluorescence flux assays

Kinetics of SthK response to cyclic nucleotides were monitored with a sequential-mixing, stopped-flow fluorescence-ensemble assay (Rusinova et al., 2014; Posson et al., 2018) based on the Tl^+-induced quenching of a liposome-encapsulated fluorescent dye (8-aminonaphthalene-1,3,6-trisulfonic acid [ANTS], disodium salt; Life Technologies). For this assay, the gel filtration was performed in 10 mM HEPES, 140 mM KNO_3, and 0.5 mM DDM, pH 7.4. To reconstitute SthK into liposomes, DOPC, POPG, and cardiolipin (Avanti Polar Lipids), dissolved in chloroform, were mixed in a 5:3:2 (wt/wt/wt) ratio and dried under constant N_2 flow in disposable glass tubes to a thin layer. Lipids were further dried overnight under vacuum and then solubilized (10 mg/ml final concentration) in reconstitution buffer (15 mM HEPES and 150 mM KNO_3, pH 7.4) in the presence of 33 mM CHAPS. ANTS was added to a final concentration of 25 mM before adding SthK (30 µg/mg lipid). Detergent removal was performed by incubating the reconstitution mixture with 0.75 g BioBeads (Bio-Rad Laboratories) for 3 h under constant agitation. Subsequently, the solution was separated from the BioBeads, sonicated for 20 s, and extruded (Mini Extruder, 0.1-µm membrane; Avanti Polar Lipids). The liposome solution was run over a PD-10 desalting column (GE Healthcare Life Sciences), equilibrated in recording buffer (10 mM HEPES and 140 mM KNO_3, pH 7.4) to remove extravesicular ANTS. For the measurements, liposomes were diluted fivefold in recording buffer to ensure a good signal/noise ratio.

All measurements were performed with a SX20 sequential-mixing, stopped-flow spectrophotometer (Applied Photophysics) at 25°C. In the first mixing step, liposomes were diluted 1:1 with recording buffer containing ligands to activate SthK. After incubating the solution for the defined times (0.015–10 s), a second 1:1 mixing step was performed with quenching buffer (10 mM HEPES, 90 mM KNO_3, and 50 mM $TlNO_3$, pH 7.4) containing ligand at the same concentration. Quenching of the ANTS fluorescence by Tl^+ was monitored above 450 nm after excitation at 360 nm. For each condition, at least eight repeats were performed. Reference measurements were performed with recording buffer instead of quenching buffer. All experiments were repeated at least three times with protein from different reconstitutions. Identical control measurements were performed with protein-free liposomes. The day-to-day performance, as seen in the rate constants, was within 20%.

To assess the time course of SthK activation by cAMP, a final concentration of 200 µM cAMP was used. Delay times after the first mixing step were varied between 15 ms and 10 s to cover a wide range of incubation times. To determine the apparent activation constant 50% effective concentration (EC_{50}) of cAMP for SthK, the concentrations of cAMP in the recording and quenching buffers varied between 0 and 400 µM. The delay time was kept constant at 2.5 s to ensure SthK was activated completely under each condition. The apparent 50% inhibition constant IC_{50} of cGMP for SthK was determined by mixing apo-SthK with 200 µM cAMP and increasing concentrations of cGMP (0–1 mM) at the same time for 2.5 s before performing the second mixing step with quenching buffer and the final cAMP/cGMP concentrations. Because we performed the reconstitution in the absence of cAMP, the SthK channels with the CNBDs facing inside of the liposomes were closed and did not contribute to the quenching kinetics.

Stopped-flow data analysis

Fluorescence quenching data were analyzed as described (Ingólfsson and Andersen, 2010; Rusinova et al., 2014; Posson et al., 2018). In brief, a stretched-exponential function (Eq. 8) was fitted to the first 100 ms of fluorescence decay (liposome size distribution and different numbers of channels per liposome do not allow for mono- or double-exponential fits):

$$F_t = F_\infty + \left(F_0 - F_\infty\right) \cdot e^{\left[-\left(\frac{t}{\tau}\right)^{\beta}\right]} \tag{8}$$

where F_t is the fluorescence at time t; F_∞ and F_0 are the final and initial fluorescence, respectively; τ is the time constant of the quenching reaction; and β is the stretched-exponential coefficient.

The rate of Tl^+ influx at 2 ms, referred to as the Tl^+ flux rate in the text, was calculated using Eq. 9 and the parameters from the stretched-exponential fits:

$$k_t = \left(\frac{\beta}{\tau}\right) \cdot \left(\frac{2\ \text{ms}}{\tau}\right)^{\beta-1} \tag{9}$$

where k_t is the rate at 2 ms in s^{-1}. This rate is dependent on many parameters, such as the number of channels per liposome, the liposomal size, the open probability of the channels, the conductance of the channels, and the rate of activation/inactivation.

To analyze the time course of SthK activation by cAMP, the averaged Tl^+ flux rates were plotted as functions of the delay time, and an exponential function was used to fit the data. The EC_{50} value was estimated by plotting the averaged Tl^+ flux rates as a function of the cAMP concentration and fitting the data with a modified Hill equation (Eq. 10) to

$$y([\text{cAMP}]) = \frac{k_{max} \cdot [\text{cAMP}]^{n_H}}{(EC_{50})^{n_H} + [\text{cAMP}]^{n_H}} \tag{10}$$

where k_{max} is the maximum rate at the saturating ligand concentration, [cAMP] is the concentration of cAMP in micromolars, EC_{50} is the concentration at half the activation in micromolars, and n_H is the Hill coefficient.

The IC_{50} value for the inhibition of SthK by cGMP in the presence of 200 µM cAMP was calculated by assuming that cGMP was a competitive antagonist of cAMP, using Eq. 11:

$$y([\text{cGMP}]_f) = \frac{y_{max}}{1 + \left(\frac{[\text{cGMP}]}{IC_{50}}\right)^s} \tag{11}$$

where y_{max} is the maximum SthK activity in the presence of only cAMP, [cGMP] is the respective concentration of cGMP in micromolars, IC_{50} is the apparent inhibition constant in micromolars, and s is the slope factor.

The IC_{50} values were used to calculate an apparent inhibition constant K_i (Eq. 12; Cer et al., 2009) based on a model similar to the one described in Eq. 5:

$$K_i = \frac{IC_{50}}{\frac{[\text{cAMP}]}{K_d} + 1} \tag{12}$$

where IC_{50} is the inhibition constant obtained from Eq. 11, [cAMP] is the concentration of cAMP present during the inhibition experiment, and K_d is the apparent dissociation constant for cAMP obtained from Eq. 6.

Electrophysiology

Single-channel recordings of SthK were performed as described previously (Thompson et al., 2008; Cheng et al., 2011) in a horizontal lipid-bilayer setup at room temperature where the cis (upper) and trans (lower) chambers were separated by a partition with a 100-µm-diameter hole (LeMasurier et al., 2001). Bilayers are painted over the hole with a smooth capillary glass stick and 6.25 mg/ml of 1,2-diphytanoyl-*sn*-glycero-3-phosphocholine dissolved in *n*-decane. The prefrozen proteoliposomes were briefly sonicated (~2 s) before application to the cis side of the bilayer. The electrophysiology buffer contained 97 mM KCl, 3 mM KOH, and 10 mM HEPES, pH 7. Ligand exchange was performed by perfusing electrophysiology buffer containing different concentrations of cAMP or cGMP into the trans chamber to measure various activity levels of SthK. cAMP-free solutions in the cis chamber ensured that we only recorded from channels with their CNBDs facing the trans chamber. Channel activity was monitored with an Axopatch 200A or B (Molecular Devices). Electrophysiology traces were filtered online at 1 kHz with an eight-pole, low-pass Bessel filter, digitized at 20 kHz (Digidata 1440A; Molecular Devices), recorded with Clampex (Molecular Devices), and analyzed with Clampfit (version 10; Molecular Devices). Amplitudes of long openings were measured manually, and the results were confirmed by all-amplitude histograms (Fig. S3). The concentration for half-maximal activation, EC_{50}, for cAMP, was determined with Eq. 10, and the apparent inhibition constant for cGMP was determined with Eq. 11. The change in open probability with the voltage was fitted with a Boltzmann function (Eq. 13):

$$\text{Po}\left(\text{V}\right) = \frac{\text{Po}_{max} - \text{Po}_{min}}{1 + e^{\left[\frac{-F \cdot z \cdot \left(\text{V} - \text{V}_{half}\right)}{R \cdot T}\right]}} + \text{Po}_{min} \tag{13}$$

where F is the Faraday constant, z is the gating charge, V_{half} is the voltage at half activation, R is the universal gas constant, T is the temperature, and Po_{max} and Po_{min} are the fitted maximum and minimum open probabilities, respectively.

Negative-stain EM imaging and analysis

3 µl of freshly prepared protein (10 µg/ml) was applied to a glow-discharged (15 mA, 1 min, easiGlow; PELCO), homemade, carbon-coated copper grid (400 mesh; Electron Microscopy Sciences) and incubated for 60 s. The grid was washed four times with double-distilled H_2O, and excess water was removed by blotting after each step. The grid was dipped into 1.5% uranyl acetate stain for 1 s, then blotted and stained again for an additional 20 s. Excessive stain was removed by blotting, and the grid was air dried for 5 min. This protocol was adapted from Ohi et al. (2004).

The prepared grids were imaged in an FEI Tecnai T12 electron microscope operated at 120 kV acceleration voltage, equipped with a Tietz F416 camera (2,048 × 2,048 pixels). Micrographs were obtained at a magnification of 49,000 with Leginon (Suloway et al., 2005), resulting in a pixel size of 3.44 Å/pixel. Particles were selected with DoG Picker (Voss et al., 2009), included in the Appion (Lander et al., 2009; Voss et al., 2010) processing package. Extracted particle images were subjected to iterative rounds of 2-D classification with RELION 2.1 (Scheres, 2012; Kimanius et al., 2016).

Online supplemental material

Fig. S1 provides a sequence alignment of SthK with CNG and HCN channels showing the homology to its eukaryotic counterparts. Fig. S2 shows the incorporation efficiency of SthK into liposomes of different lipid compositions, as assessed by SDS-PAGE, and corroborates the differences in activity presented in Fig. 2 (A and B). In Fig. S3, all-amplitude histograms from single-channel bilayer recordings are presented, corresponding to Fig. 2 D. Fig. S4 provides additional single-channel traces and fluorescence-quenching kinetics. Fig. S4 A shows the differential activation of SthK by cAMP and cGMP, corresponding to Fig. 4. The quenching kinetics in Fig. S4 B demonstrate that no Tl^+ influx was observed in the empty liposomes and in the absence of cAMP, and it relates to Fig. 3.

Results

Expression and purification of recombinant SthK

The full-length gene for SthK was cloned from the genome of *S. thermophila* into the pCGFP-BC vector, which enables expression of recombinant proteins as C-terminal GFP–His_8 fusion proteins in *E. coli* (Kawate and Gouaux, 2006). A series of constructs with N- and C-terminal truncations was tested for optimal protein expression. $SthK_{\Delta 421–430}$ led to the highest expression, as assessed by whole-cell fluorescence measurements. Small-scale expression and purification, followed by fluorescence-detection size-exclusion chromatography was used to screen various detergents for extraction of the channel from membranes (Kawate and Gouaux, 2006). Using DDM for extraction and purification resulted in a homogenous protein peak during gel-filtration chromatography and a single band on SDS-PAGE. For further protein production, the gene for GFP and four of the eight histidines from the purification tag were deleted from the plasmid with no obvious, adverse effects on channel expression, purification, and stability (protein yield from 4-liter bacterial culture was ~7 mg SthK; Fig. 1 B). All the results presented here used that final expression construct, and we refer to it as SthK for convenience.

Because SthK runs close to the monomer size during SDS-PAGE, we performed cross-linking experiments with glutaraldehyde, using the purified protein in DDM to analyze the oligomeric state of the protein. SthK is readily cross-linked by 0.12% glutaraldehyde (2-min incubation time at 37°C) and appears only as a tetramer on SDS-PAGE (Fig. 1 B, lane 2). Negative-stain, single-particle EM revealed uniformly distributed particles on the grid, with only minor aggregation (Fig. 1 C), closely corresponding to the presumed size of a channel tetramer (75 × 100 Å, as measured from the structure of HCN1; Lee and MacKinnon, 2017). 2-D class averages generated from single-particle processing and analysis closely resembled those of other cyclic nucleotide–modulated channel structures solved with cryo-EM (James et al., 2017; Li et al., 2017), suggesting that SthK is a good candidate for high-resolution structural studies with single-particle cryo-EM (Fig. 1 D).

Purified SthK activity in liposomal ^{86}Rb uptake assays

To screen for function and favorable conditions for channel activity, we used a largely qualitative $^{86}Rb^+$ flux assay (Nimigean, 2006), in which SthK is reconstituted in liposomes loaded with a high concentration of KCl, and we evaluated the ability of the protein to pass K^+ across the membrane and take up trace amounts of externally added $^{86}Rb^+$. Initial experiments with SthK, reconstituted in a 3:1 mixture of POPE:POPG (Cheng et al., 2011), led to little $^{86}Rb^+$ uptake, indicating extremely low activity, even in the presence of 200 µM cAMP. However, reconstitution of SthK in liposomes containing lipids such as DOPC, POPG, and cardiolipin, which are more prevalent in spirochetes (Livermore and Johnson, 1974; Reddy et al., 2013), yielded more robust cAMP-dependent activity (Fig. 2, A and B). The various lipid compositions we tested in this work did not affect SthK-incorporation efficiencies, as analyzed by SDS-PAGE (Fig. S2), and, accordingly, the differences in $^{86}Rb^+$ uptake in Fig. 2 B likely resulted from differences in protein activity. Unlike the studies for SthK expressed in oocytes (Brams et al., 2014), cGMP also supports $^{86}Rb^+$ uptake in SthK liposomes, suggesting that cGMP may also be able to activate SthK, although less efficiently than cAMP does (Fig. 2 A).

Single-channel properties of purified SthK channels in lipid bilayers

Reconstitution of SthK in the same DOPC:POPG:cardiolipin lipid mixture that mediated robust $^{86}Rb^+$ uptake allowed observation of single-channel activity in horizontal lipid bilayers (Fig. 2 C and Fig. S4 A). The single-channel currents were asymmetric: the amplitude of the outward currents was lower, but their single-channel open probability was higher, and we observed robust channel openings. In contrast, the inward currents appeared flickery and were very brief (Fig. 2 C). The orientation of the channel was determined by the current response to perfusions with either no cyclic nucleotides or saturating cAMP concentrations ([cAMP] ≥ 100 µM). The effect of cAMP was fully reversible.

The EC_{50} of the channel response to cAMP was ~17 µM (at 100 mV; Fig. 2 E), comparable to what was previously measured

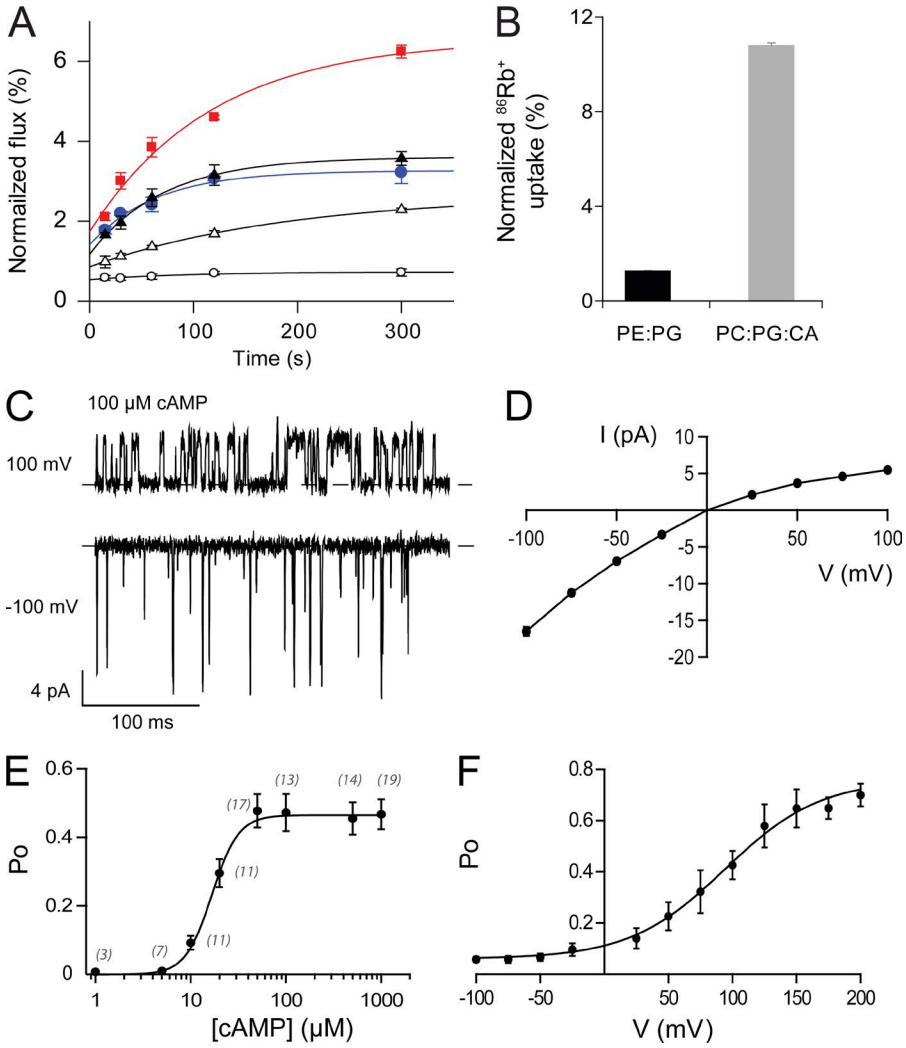

Figure 2. **Characterization of SthK channel activity. (A)** Normalized $^{86}Rb^+$ flux through SthK (reconstituted in 5:3:2 DOPC:POPG:cardiolipin) in the presence of 200 µM cAMP (red squares), cGMP (blue circles), both cAMP and cGMP (black triangles), and without cyclic nucleotides (open triangles). Flux through empty liposomes (open circles) is shown as a reference. All flux values are normalized to the maximum uptake recorded in the presence of valinomycin. Bars represent means ± SEM for three separate experiments. **(B)** SthK channel activity represented by the maximum achieved $^{86}Rb^+$ uptake through SthK reconstituted in liposomes made from 3:1 POPE:POPG (PE:PG) or 5:3:2 DOPC:POPG:cardiolipin (PC:PG:CA), as indicated, in the presence of 200 µM cAMP. Bars represent means ± SEM for three separate experiments. **(C)** Representative single-channel recordings of SthK in 0.1 mM intracellular cAMP. **(D)** I-V relationship of SthK single-channel current amplitude at 100 µM cAMP. **(E)** Open probability of SthK at 100 mV as a function of the cAMP concentration. Fitting the data with Eq. 10 yields an apparent activation constant of EC_{50} = 17 µM and a Hill coefficient of n_H = 3. The number of repeats is indicated beside each data point. **(F)** Open probability of SthK in the presence of 500 µM cAMP as function of the membrane potential. The line indicates the fit according to Eq. 13, leading to z = 0.8 and V_{half} = 87 mV, Po_{max} = 0.65, and Po_{min} = 0.05. Symbols and error bars in D–F represent means ± SEM from at least three separate bilayers.

in oocytes (EC_{50} ≈ 4 µM; Brams et al., 2014). No channel activity was observed in the absence of cAMP, and the open probability increased to a maximum of only ~0.2–0.5 at saturating cAMP and at depolarized voltage (100 mV; Fig. 2, E and F), suggesting that although cAMP is necessary and sufficient for channel activation, cAMP alone cannot fully open the channel. Patch-clamp recordings of SthK expressed in *X. laevis* oocytes showed very similar single-channel characteristics (single-channel conductance and rectification) but revealed an open probability of Po ≈ 0.14 (at 100 mV), which is within the range of open probabilities that we observed. The small differences between this study and that of Brams et al. (2014) may arise from the different membrane compositions between the two setups, possible posttranslational modifications, and slightly different protein constructs.

The large difference in SthK activity between 100 and −100 mV seen in Fig. 2 C indicates that the activity of SthK is voltage dependent. We measured the open probability as a function of the membrane potential (Fig. 2 F) and found that the Po increased with increased depolarization, with a voltage dependence of z = 0.8 and V_{half} = 87 mV in saturating cAMP. The voltage dependence of SthK was more pronounced than that observed for CNG channels (z ≈ 0.2; Benndorf et al., 1999) but was smaller and of the opposite polarity from what was observed for HCN channels (z ≈ −6; Santoro et al., 1998). Furthermore, in contrast to HCN channels, voltage alone was not able to open the channel in the absence of cAMP.

The study by Brams et al. (2014) reported a weak, outward rectification of the macroscopic current recorded from oocytes. That may appear to contrast with our analysis of the single-channel current amplitudes, which clearly showed that SthK is a strongly inwardly rectified channel (I = 4.5 and 16 pA at 100 and −100 mV, respectively; Fig. 2 D). However, an examination of the voltage-dependent, single-channel open probabilities (Fig. 2 F) revealed that at 100 mV, where the single-channel amplitude is small, the open probability was much higher than that at −100 mV, where the single-channel amplitude was larger (i.e., Po = 0.45 for 100 mV and Po = 0.06 at −100 mV). Because macroscopic current is a function of the product between open probability and single-channel current amplitude and the open probabilities at positive voltages are one order of magnitude larger than those at negative voltages (Fig. 2 F), the main determinant of the size of the macroscopic current is the open probability. That yields a weakly outwardly rectifying macroscopic current and provides an explanation at the single-channel level for the data reported by Brams et al. (2014).

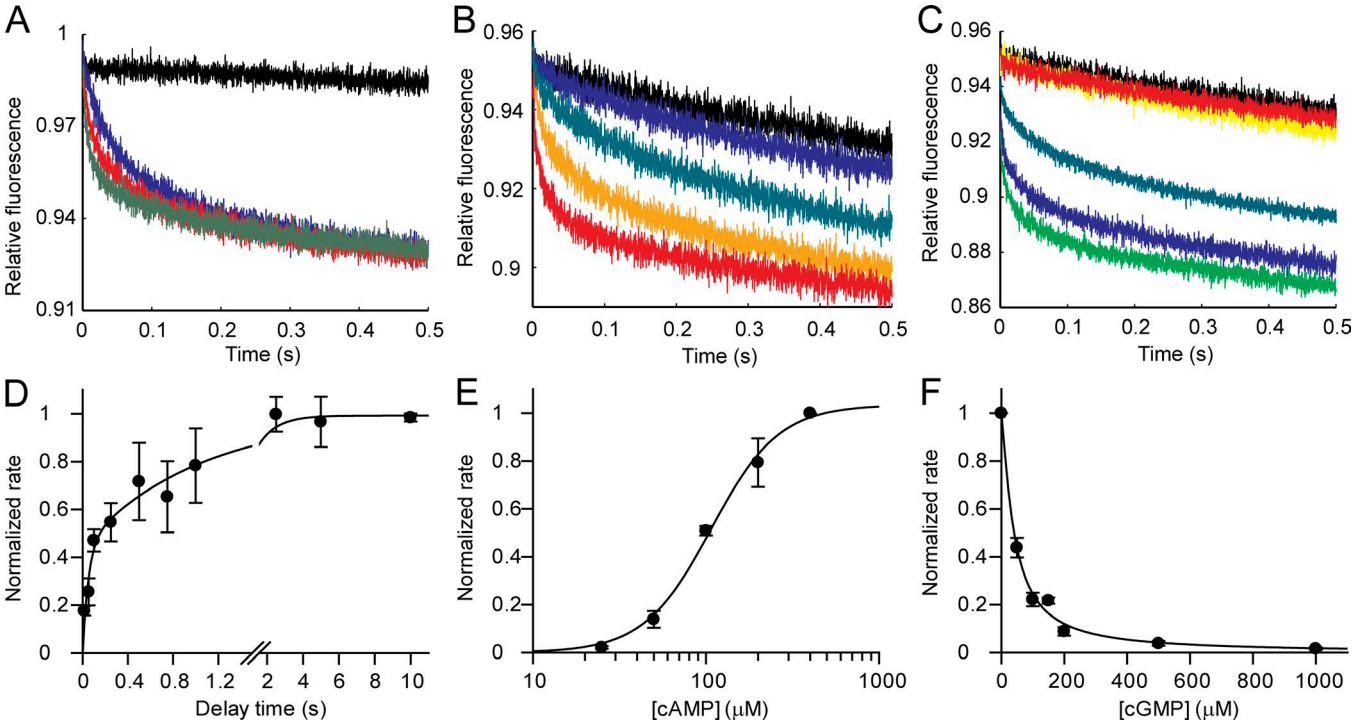

Figure 3. **Kinetics of SthK activation by cAMP and inhibition by cGMP. (A)** Fluorescence decay traces as a measure of channel activity in the stopped-flow Tl^+ flux assay after incubating the SthK liposomes with 200 μM cAMP for 15 ms (blue), 100 ms (red), and 5 s (green). 0 μM cAMP is in black. The corresponding flux rates (Eq. 9) as a function of activation time are shown in D. **(B)** Fluorescence decay traces from SthK liposomes incubated for 2.5 s with cAMP over a range of concentrations (0, 25, 50, 100, and 400 μM from top to bottom). The corresponding flux rates as a function of the cAMP concentration are shown in E. **(C)** Fluorescence decay traces from SthK liposomes incubated with 200 μM cAMP and increasing concentrations of cGMP for 2.5 s (0 μM [green], 25 μM [blue], 100 μM [turquoise], 500 μM [yellow], and 1,000 μM [red]). No cyclic nucleotides (black). The corresponding flux rates as a function of the cGMP concentration are shown in F. **(D)** The activation time course is best fitted with a sum of two exponentials (line through symbols) with time constants of $\tau_1 \approx 0.05$ s (amplitude 0.45) and $\tau_2 \approx 1.04$ s (amplitude 0.55). **(E)** A fit with Eq. 10 yields an EC_{50} of ~100 μM (line through symbols) and a Hill coefficient of 2.2 ± 0.3. **(F)** The apparent inhibition constant was determined using Eq. 11 (line through symbols) and yields an IC_{50} of 40 μM, from which the K_i of 6 μM was calculated (Eq. 12; Table 1). (D–F) Rates were normalized to the maximum value, and symbols and error bars represent means ± SEM for three experiments.

The low open probability of SthK at 0 mV diminishes the likelihood of obtaining an open-state structure. However, mutants with increased open probability at 0 mV, together with analysis of selected class averages, may help identify open conformations. Indeed, it has been shown previously (Hite and MacKinnon, 2017) that as little as 8% of all usable particles is sufficient for detecting a different conformation in single-particle cryo-EM studies.

Activation kinetics of SthK

One major difference between eukaryotic HCN and CNG channels is that CNG channels activate much faster upon cyclic nucleotide application than HCN channels do (Nache et al., 2006; Kusch et al., 2010). The mechanism responsible for that difference is not yet understood. We investigated the kinetics of SthK channel activation by examining nonequilibrium properties of SthK using a fluorescence-based, stopped-flow flux assay with millisecond time resolution (Rusinova et al., 2014; Posson et al., 2018).

We determined the SthK activation time course by incubating the channel with saturating concentrations of cAMP (200 μM) for various amounts of time (0.015–10 s) and measured the activity. The rates extracted from fitting the quenching time courses (Fig. 3 A) increased biphasically over several seconds ($\tau_1 \approx 0.05$ and $\tau_2 \approx 1.04$ s in the presence of 200 μM cAMP; Fig. 3 D). The maximum activation was reached after 2 s, and no inactivation was observed within the monitored time range (10 s). That is in agreement with single-channel recordings that allow for monitoring stable, single-channel activity, with no evidence of inactivation, from minutes to hours. A dose–response experiment in which the SthK activity was measured in different cAMP concentrations (after incubating for 2.5 s to ensure maximal activation; Fig. 3, B and E) yielded a lower apparent affinity for cAMP (EC_{50} = 107 μM) than that found in bilayers (17 μM; Fig. 2 E). It is possible that the lack of voltage across the liposomal membrane or the different experimental conditions between lipid-bilayer recordings and the liposomal flux assays (such as different permeant ions, different sensitivities in the readout, single-channel vs. ensemble measurements) contributed to the lower apparent affinity measured in the flux assays.

SthK activation by cGMP

The flux assays (Fig. 2, A and B) provided a first indication that cGMP also activates SthK, albeit to a much lesser extent than cAMP does. Application of solutions containing high concentrations of cGMP dramatically lowers the open probability of single-SthK channels previously activated by saturating cAMP concentrations, but it does not abolish the activity completely

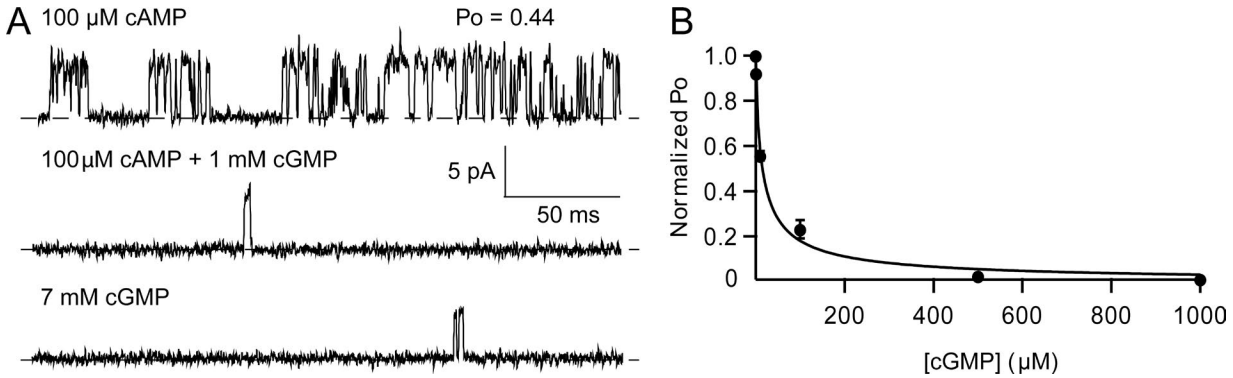

Figure 4. **cGMP inhibits cAMP-dependent channel activity. (A)** Representative single-channel traces of SthK at 100 mV in the presence of 100 µM cAMP (top trace). Addition of 1 mM cGMP (middle trace) significantly, and reversibly, reduces channel activity. Application of only cGMP (bottom trace) leads to low but nonzero channel activity. **(B)** Inhibition of preactivated SthK (by 100 µM cAMP) with increasing concentrations of cGMP. All data analyzed are from recordings at 100 mV. Data are fitted using Eq. 11, giving an IC_{50} of 16 µM. Symbols and error bars represent means ± SEM for three experiments.

(Fig. 4 A and Fig. S4). In the absence of cyclic nucleotides, no channel activity was observed (Fig. S4 A).

High concentrations of cGMP alone yielded a similarly low, but nonzero, open probability when applied in the presence of saturating cAMP (Fig. 4 A), suggesting that cGMP indeed binds to the channel, replacing cAMP in the ligand-binding pocket and also activates the channel, albeit very poorly. This observation is in agreement with our $^{86}Rb^+$ uptake experiments (Fig. 2, A and B). Unfortunately, the extremely low activity does not allow for an accurate measurement of the open probability in cGMP or the determination of an EC_{50} value. However, we were able to measure an inhibition dose–response by measuring the open probability of the channel upon addition of increasing concentrations of cGMP in the presence of saturating cAMP concentrations (Fig. 4 B). The cGMP concentration required to inhibit cAMP-induced SthK activity by 50% was 15 µM (in 100 µM cAMP; Fig. 4 B), yielding an apparent inhibition constant of ∼4 µM at 100 mV (Eq. 12).

We also tested cGMP inhibition with the stopped-flow assay by exposing SthK channels to 200 µM cAMP and increasing concentrations of cGMP (Fig. 3, C and F; and Fig. S4 B). Under these conditions, the IC_{50} for cGMP is 40 µM, which leads to an apparent inhibition constant (Eq. 12) of 6 µM, comparable to the value that we obtained from bilayer experiments ($K_i \approx 4$ µM). The concentrations of cGMP required to inhibit SthK channels were lower than the concentrations of cAMP required to activate them, suggesting a higher affinity for cGMP binding compared with cAMP. At the same time, cGMP activates SthK much less efficiently than cAMP does. To further probe the mechanism behind the different cGMP and cAMP effects on SthK, we performed ligand-binding assays.

Purified SthK specifically binds cyclic nucleotides

We measured binding of 8-NBD-cAMP (fcAMP), a fluorescent analogue of cAMP, to SthK reconstituted in amphipols (A8–35) because apo-SthK in detergent is prone to aggregation. fcAMP has previously been used successfully to characterize other cAMP-binding proteins (Kraemer et al., 2001; Cukkemane et al., 2007; Altieri et al., 2008; Brelidze et al., 2009; Chen et al., 2013). Upon titration of fcAMP with increasing concentrations of SthK, we observed an increase in the NBD fluorescence (Fig. 5 A), indicating binding of the ligand. The calculated K_d value for fcAMP was 0.6 ± 0.1 µM (Table 1). That value is ∼40 times higher than that reported for the isolated CNBD of MloK1, another prokaryotic cyclic nucleotide–modulated channel ($K_d \approx 15.9 \pm 2.7$ nM for fcAMP; Cukkemane et al., 2007) but is closer to those measured for isolated CNBDs of eukaryotic channels (0.1–1.5 µM; Lolicato et al., 2011; Goldschen-Ohm et al., 2016; and 5 µM for HCN4; Akimoto et al., 2014). The K_d for 8-NBD-cGMP (fcGMP), a fluorescent analogue of cGMP, was determined in a similar experiment to be 2.7 ± 0.5 µM, somewhat lower than the value obtained for fcAMP.

Specific binding of cAMP and cGMP was determined with fluorescence-based competition assays in which binding of fcAMP to SthK was measured in the presence of increasing concentrations of nonfluorescent cAMP or cGMP (Fig. 5 B). Estimated K_d values for cAMP and cGMP were in the range of 20–50 µM (Eq. 6), indicating that the two ligands may interact with SthK with lower affinity than the fluorescent ligands (Table 1). The increased affinity for the fluorescent ligands may originate from the NBD moiety, which has been described before to increase the affinity of cyclic nucleotides (Cukkemane et al., 2007), probably by establishing additional interactions with the protein. Despite the many simplifying assumptions used to determine the apparent binding parameters from these assays (Eqs. 1, 2, 3, 4, 5, and 6), they nevertheless showed that cAMP and cGMP interact specifically and with similar affinities with SthK because both ligands are able to compete with fcAMP for the binding site in the CNBD over the same concentration range. Thus, it appears that the lower SthK opening probability in the presence of cGMP compared with cAMP cannot be explained by a lower binding affinity for cGMP. Rather, it appears that cGMP binding may not be able to support the conformational change to an open state as efficiently as cAMP can.

Discussion

In this work, we present the functional characterization of a purified CNG channel under defined conditions. We optimized the expression and purification of SthK, a channel that shares

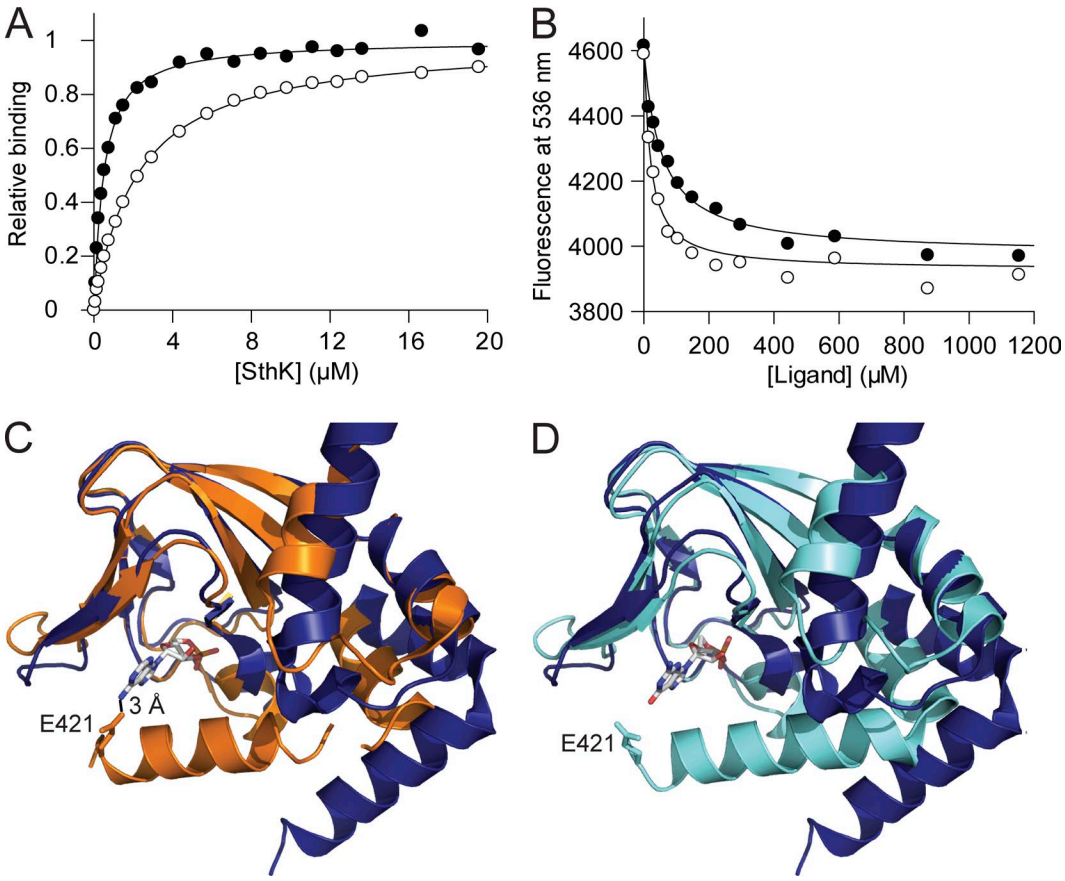

Figure 5. **Interaction of cAMP and cGMP with SthK. (A)** Titration of 0.1 μM fcAMP (closed circles) or fcGMP (open circles) with SthK in A8-35; lines represent fits according to Eq. 4, giving K_d values of 0.4 μM and 2 μM, respectively. The data presented are from a single measurement; averaged values from three separate titrations are listed in Table 1. **(B)** Representative titration of the SthK · fcAMP complex with increasing concentrations of cAMP (closed circles) or cGMP (open circles). The K_d values for the unlabeled cyclic nucleotides obtained from these titrations according to Eq. 6 are 50 ± 8 μM for cAMP and 19 ± 4 μM for cGMP. Averaged values from three competition experiments are given in Table 1. **(C and D)** Overlay of the CNBDs of HCN2 (apo [blue], 5JON [Goldschen-Ohm et al., 2016]) and SthK in complex with cAMP (orange, 4D7T [Kesters et al., 2015]) in C, and the same HCN2 and SthK in complex with cGMP (cyan, 4D7S [Kesters et al., 2015]) in D. The figures were prepared using PyMol (http://www.pymol.org). The ligands cAMP (C) and cGMP (D) are shown in stick representation in CPK colors. Only E421 is shown to indicate an interaction with cAMP (C) but not with cGMP (D).

high sequence similarity with eukaryotic CNG as well as with HCN channels and that has been previously identified as a possible homologue for CNG channels (Brams et al., 2014; Kesters et al., 2015). The SthK channel protein is stable in detergent, amphipol, and liposomes and is amenable to single-channel bilayer recordings, ligand-binding assays, a Tl^+ flux-stopped flow assay, and negative-stain EM, making it a great model system for investigating the molecular mechanism of CNG/HCN channel function and regulation.

Sequence alignments with CNG and HCN channels reveal that, overall, SthK shares more similarities with HCN channels, especially in the S4 voltage-sensor region and the CNBDs. On the other hand, there are regions, such as the pore helix and the C-linker, where more similarity is found with CNG channels (Fig. S1). Our first observations were that cAMP was necessary and sufficient to activate purified SthK channels, although only partially, even under saturating cAMP, and that depolarization increased the open probability. The direct activation of the channel upon cyclic nucleotide binding and the polarity of the voltage that increases the channel activity are features that are similar to eukaryotic CNG-type channels, rather than HCN channels (Benndorf et al., 1999). However, the voltage-dependence of SthK is approximately fourfold larger than that of CNG channels, but it is still approximately eightfold less, and of opposite polarity, than the voltage dependence of HCN and sea urchin HCN channels (Gauss et al., 1998; Ludwig et al., 1998).

Examination of the sequence reveals that SthK and CNG channels have a significantly shorter S4 than HCN channels. The high-resolution structure of HCN1 showed an unusually long S4 helix with 8–10 positively charged residues, and these features were used to interpret the strong dependence of the HCN channel activity on hyperpolarization (Lee and MacKinnon, 2017). The SthK S4 has fewer charged residues than the CNG channels, but it shows a more pronounced voltage dependence, suggesting that the number of positively charged residues in S4 alone does not fully account for the voltage gating, as previously proposed (Tang and Papazian, 1997; Carvalho-de-Souza and Bezanilla, 2018). A direct comparison of the structures of HCN1 and Tax-4 raises the possibility that the coordination of the charges, the shape of S4 (straight vs. bent helix, respectively), and the orientation

Table 1. **Numerical values of the interaction between SthK and cyclic nucleotides**

Cyclic nucleotide assay	K_d (μM)	SEM
Direct binding assay		
fcAMP	0.6	0.1
fcGMP	2.7	0.5
Competition assay		
cAMP	36	12
cGMP	28	9
Activation of SthK by cAMP	**EC_{50} (μM)**	**SEM**
Bilayer recordings	17	0.8
Stopped flow	107	8
Inhibition of SthK by cGMP	**K_i (μM)**	**SEM**
Bilayer recordings	4	0.5
Stopped flow	6	0.7

Table 1 provides the numerical values obtained from the binding and activation studies of SthK. K_i values for cGMP inhibition were calculated according to Eq. 12. The listed values are correlated with the data shown in Figs. 2, 3, 4, and 5 and represent means ± SEM for at least three independent measurements.

of S4 relative to the pore may be more important for efficient voltage sensing.

In spite of the large, functional similarity with CNG channels, neither cAMP nor cGMP can fully activate SthK. cAMP alone can activate the channel but only to a small fraction (Po ≈ 0.1 at 0 mV), making it an inefficient partial agonist. Interestingly, although previously reported to be an antagonist, cGMP is also able to open the channel albeit to very low levels (Po < 0.003), making cGMP an extremely poor partial agonist. Such a differential effect of these two ligands has been observed previously, in particular for CNGA1, where cGMP is significantly more efficient in activating the channel compared with cAMP (Kaupp and Seifert, 2002; Craven and Zagotta, 2006). It has been hypothesized that ligand selectivity can originate from different intrinsic ligand-binding affinities, different efficacies, or a combination of both (Kaupp and Seifert, 2002; Craven and Zagotta, 2006). Our data indicate that the affinities for both ligands are very similar, in the range of ∼20–50 μM, as determined from a competition assay, suggesting that, in this case, the differences in efficacy between cGMP and cAMP do not arise from different intrinsic binding affinities to the ligand binding pocket of SthK.

It is important to point out that, in our binding assays, we actually determined the affinities of cAMP and cGMP for the closed state of SthK, because neither ligand efficiently promotes the conformational change to the open state (both cAMP- and cGMP-bound SthK display very low to negligible activity at 0 mV). Because the ligands bind to the CNBD in an apo conformation, we overlaid the only available structure of an apo CNBD (of HCN2, navy in Fig. 5, C and D; Goldschen-Ohm et al., 2016) with those of SthK bound with ligands (orange and cyan in Fig. 5, C and D; Kesters et al., 2015) to investigate the differential interactions between the ligands and the binding site in those states. The apo, "resting" CNBD structure differs from the ligand-bound, "activated" CNBD structures mainly in the different orientation of the C helix, which interacts closely with the ligand in the bound structures and swings away from the ligand-binding pocket in the apo state (compare the navy with the orange and the cyan C helices in Fig. 5, C and D). The main coordination of both cyclic nucleotides with the ligand-binding pocket of the apo CNBD (navy, Fig. 5, C and D) occurs via their identical ribose and phosphate groups, whereas no interaction was seen with the C helix, which may explain the similar binding affinities between cAMP and cGMP (Gordon and Zagotta, 1995; Varnum et al., 1995; Gordon et al., 1996; Zhou and Siegelbaum, 2007). Thus, the much higher efficiency with which cAMP binding opens the SthK channel must lie in the set of favorable interactions cAMP makes with the binding pocket of the "activated" CNBD. These differences likely arise from differences in their purine bases. An example of such an interaction that cAMP may favor, whereas cGMP may not, is with E421, the last-resolved residue in the crystal structures (Fig. 5, C and D). The positively charged amino group (the substituent at position 6) of cAMP is close to the carboxylate group of E421 (∼3 Å), whereas the carbonyl oxygen of the keto group (at position 6 of the purine ring) could be more repellent toward this residue (Zagotta et al., 2003; Clayton et al., 2004; Cukkemane et al., 2011; Saponaro et al., 2014). The existing structures appear consistent with the functional data we observed, with the caveat that the C termini of the C helices are slightly different than in our construct (Fig. S1) and are also not well defined in the crystal structures, indicating some flexibility in the region and some uncertainty about the specific residues that are responsible for the differential interactions between the two ligands. In addition, these structures are of isolated C-linker/CNBDs, and one can only speculate about the effects on the pore. Thus, high-resolution structures of full-length SthK will be necessary to elucidate the diverging effects of cAMP and cGMP on channel gating. Our negative-stain EM analysis indicates that SthK is a promising candidate for high-resolution, single-particle cryo-EM structure determination. Together with our functional data, this will help to increase the understanding of CNG channel gating at the molecular level.

Measurements of the activation kinetics in SthK revealed two activation phases of ∼100 ms and ∼2 s. Biphasic activation has been seen before for CNG channels (Nache et al., 2006) and is believed to reflect the presence of multiple states in the channel-activation pathway. The fast component observed for SthK is within the range of activation times seen for CNG channels (milliseconds). In contrast, the slow-activation component observed for SthK is more reminiscent of HCN channels. For instance, HCN2, the pacemaker channel, responds to cAMP binding with time constants of seconds (Kusch et al., 2010). Further experiments will be necessary to dissect the mechanism responsible for SthK activation to occur over such different time scales.

In summary, the results presented here show that SthK is a good model system for analyzing different aspects of CNG and HCN channel function in molecular detail. Similar to CNG channels, SthK requires binding of cyclic nucleotides to the CNBD to open and thus can be used as a model to understand gating of CNG channels. The modulation of SthK channel function by

depolarization is more pronounced than in CNG channels, but this might turn out to be beneficial for understanding the effect of voltage on cAMP-mediated gating. Maximum activation of SthK by cAMP occurs within 1–2 s and, thus, is similar to the modulation of HCN2 by cAMP. Hence, the bacterial SthK channel combines interesting features of both eukaryotic CNG and HCN channels, and in light of emerging high-resolution structural data on these channels, our data will provide a good framework for interpreting conformational changes during gating.

Conclusion

In this work, we present a method for obtaining highly pure and homogenous recombinant SthK channel. Our expression and purification protocol yields several milligrams of pure channel, and we show that SthK is amenable to a variety of biophysical and functional assays. The purified channel is active, and its activity is dependent on the presence and type of cyclic nucleotide. Compared with other homologous bacterial channels, SthK is unique because it displays currents that can be analyzed at the single-channel level, shows differential regulation by cAMP and cGMP, and has cAMP/cGMP activation/binding affinities similar to those reported for eukaryotic channels. Purified SthK specifically binds cAMP and cGMP with similar micromolar affinities, despite their very different efficiencies of opening the channel, allowing us to differentiate between two mechanisms of ligand discrimination. Collectively, SthK is a useful tool for performing more specific structural, biophysical, and biochemical studies to increase our understanding about ligand binding and activation in HCN and CNG channels.

Acknowledgments

This work was supported in part by the National Institutes of Health (NIH) grants (R01GM124451 and R01GM088352) to C.M. Nimigean and the Deutsche Forschungsgemeinschaft (SCHM 3198/1-1) to P.A.M. Schmidpeter. Some of this work was performed at the Simons Electron Microscopy Center and National Resource for Automated Molecular Microscopy located at the New York Structural Biology Center, supported by grants from the Simons Foundation (SF349247), NYSTAR, and the NIH National Institute of General Medical Sciences (GM103310).

The authors declare no competing financial interests.

Author contributions: V. Uphadyay performed initial expression and purification screens and the radioactive flux assays. V. Uphadyay, P.A.M. Schmidpeter, and J. Rheinberger optimized protein expression. J. Rheinberger collected and analyzed EM data. X. Gao collected and analyzed the electrophysiology data. P.A.M. Schmidpeter collected and analyzed the binding and stopped-flow data. All authors contributed to the experimental design, manuscript writing, and agreed with the final version of the manuscript.

Sharona E. Gordon served as editor.

Submitted: 9 February 2018
Accepted: 9 April 2018

References

Accili, E.A., C. Proenza, M. Baruscotti, and D. DiFrancesco. 2002. From funny current to HCN channels: 20 years of excitation. *News Physiol. Sci.* 17:32–37.

Akimoto, M., Z. Zhang, S. Boulton, R. Selvaratnam, B. VanSchouwen, M. Gloyd, E.A. Accili, O.F. Lange, and G. Melacini. 2014. A mechanism for the auto-inhibition of hyperpolarization-activated cyclic nucleotide-gated (HCN) channel opening and its relief by cAMP. *J. Biol. Chem.* 289:22205–22220. https://doi.org/10.1074/jbc.M114.572164

Altieri, S.L., G.M. Clayton, W.R. Silverman, A.O. Olivares, E.M. De la Cruz, L.R. Thomas, and J.H. Morais-Cabral. 2008. Structural and energetic analysis of activation by a cyclic nucleotide binding domain. *J. Mol. Biol.* 381:655–669. https://doi.org/10.1016/j.jmb.2008.06.011

Benndorf, K., R. Koopmann, E. Eismann, and U.B. Kaupp. 1999. Gating by cyclic GMP and voltage in the α subunit of the cyclic GMP-gated channel from rod photoreceptors. *J. Gen. Physiol.* 114:477–490. https://doi.org/10.1085/jgp.114.4.477

Biel, M., C. Wahl-Schott, S. Michalakis, and X. Zong. 2009. Hyperpolarization-activated cation channels: from genes to function. *Physiol. Rev.* 89:847–885. https://doi.org/10.1152/physrev.00029.2008

Brams, M., J. Kusch, R. Spurny, K. Benndorf, and C. Ulens. 2014. Family of prokaryote cyclic nucleotide-modulated ion channels. *Proc. Natl. Acad. Sci. USA.* 111:7855–7860. https://doi.org/10.1073/pnas.1401917111

Brelidze, T.I., A.E. Carlson, and W.N. Zagotta. 2009. Absence of direct cyclic nucleotide modulation of mEAG1 and hERG1 channels revealed with fluorescence and electrophysiological methods. *J. Biol. Chem.* 284:27989–27997. https://doi.org/10.1074/jbc.M109.016337

Carvalho-de-Souza, J.L., and F. Bezanilla. 2018. Nonsensing residues in S3-S4 linker's C terminus affect the voltage sensor set point in K^+ channels. *J. Gen. Physiol.* 150:307–321. https://doi.org/10.1085/jgp.201711882

Cer, R.Z., U. Mudunuri, R. Stephens, and F.J. Lebeda. 2009. IC50-to-Ki: a web-based tool for converting IC50 to Ki values for inhibitors of enzyme activity and ligand binding. *Nucleic Acids Res.* 37(Web Server issue, Web Server):W441-5. https://doi.org/10.1093/nar/gkp253

Chen, H., T. Tsalkova, O.G. Chepurny, F.C. Mei, G.G. Holz, X. Cheng, and J. Zhou. 2013. Identification and characterization of small molecules as potent and specific EPAC2 antagonists. *J. Med. Chem.* 56:952–962. https://doi.org/10.1021/jm3014162

Cheng, W.W., J.G. McCoy, A.N. Thompson, C.G. Nichols, and C.M. Nimigean. 2011. Mechanism for selectivity-inactivation coupling in KcsA potassium channels. *Proc. Natl. Acad. Sci. USA.* 108:5272–5277. https://doi.org/10.1073/pnas.1014186108

Chiu, P.-L., M.D. Pagel, J. Evans, H.-T. Chou, X. Zeng, B. Gipson, H. Stahlberg, and C.M. Nimigean. 2007. The structure of the prokaryotic cyclic nucleotide-modulated potassium channel MloK1 at 16 A resolution. *Structure.* 15:1053–1064. https://doi.org/10.1016/j.str.2007.06.020

Clayton, G.M., W.R. Silverman, L. Heginbotham, and J.H. Morais-Cabral. 2004. Structural basis of ligand activation in a cyclic nucleotide regulated potassium channel. *Cell.* 119:615–627. https://doi.org/10.1016/j.cell.2004.10.030

Craven, K.B., and W.N. Zagotta. 2006. CNG and HCN channels: two peas, one pod. *Annu. Rev. Physiol.* 68:375–401. https://doi.org/10.1146/annurev.physiol.68.040104.134728

Cukkemane, A., B. Grüter, K. Novak, T. Gensch, W. Bönigk, T. Gerharz, U.B. Kaupp, and R. Seifert. 2007. Subunits act independently in a cyclic nucleotide-activated K(+) channel. *EMBO Rep.* 8:749–755. https://doi.org/10.1038/sj.embor.7401025

Cukkemane, A., R. Seifert, and U.B. Kaupp. 2011. Cooperative and uncooperative cyclic-nucleotide-gated ion channels. *Trends Biochem. Sci.* 36:55–64. https://doi.org/10.1016/j.tibs.2010.07.004

DiFrancesco, D. 1986. Characterization of single pacemaker channels in cardiac sino-atrial node cells. *Nature.* 324:470–473. https://doi.org/10.1038/324470a0

Flynn, G.E., K.D. Black, L.D. Islas, B. Sankaran, and W.N. Zagotta. 2007. Structure and rearrangements in the carboxy-terminal region of SpIH channels. *Structure.* 15:671–682. https://doi.org/10.1016/j.str.2007.04.008

Gauss, R., R. Seifert, and U.B. Kaupp. 1998. Molecular identification of a hyperpolarization-activated channel in sea urchin sperm. *Nature.* 393:583–587. https://doi.org/10.1038/31248

Goldschen-Ohm, M.P., V.A. Klenchin, D.S. White, J.B. Cowgill, Q. Cui, R.H. Goldsmith, and B. Chanda. 2016. Structure and dynamics underlying elementary ligand binding events in human pacemaking channels. *eLife.* 5:5. https://doi.org/10.7554/eLife.20797

Gordon, S.E., and W.N. Zagotta. 1995. Localization of regions affecting an allosteric transition in cyclic nucleotide-activated channels. *Neuron.* 14:857–864. https://doi.org/10.1016/0896-6273(95)90229-5

Gordon, S.E., J.C. Oakley, M.D. Varnum, and W.N. Zagotta. 1996. Altered ligand specificity by protonation in the ligand binding domain of cyclic nucleotide-gated channels. *Biochemistry.* 35:3994–4001. https://doi.org/10.1021/bi952607b

Heginbotham, L., L. Kolmakova-Partensky, and C. Miller. 1998. Functional reconstitution of a prokaryotic K+ channel. *J. Gen. Physiol.* 111:741–749. https://doi.org/10.1085/jgp.111.6.741

Hite, R.K., and R. MacKinnon. 2017. Structural Titration of Slo2.2, a Na^+-Dependent K^+ Channel. *Cell.* 168:390–399.e11. https://doi.org/10.1016/j.cell.2016.12.030

Ingólfsson, H.I., and O.S. Andersen. 2010. Screening for small molecules' bilayer-modifying potential using a gramicidin-based fluorescence assay. *Assay Drug Dev. Technol.* 8:427–436. https://doi.org/10.1089/adt.2009.0250

James, Z.M., and W.N. Zagotta. 2018. Structural insights into the mechanisms of CNBD channel function. *J. Gen. Physiol.* 150:225–244. https://doi.org/10.1085/jgp.201711898

James, Z.M., A.J. Borst, Y. Haitin, B. Frenz, F. DiMaio, W.N. Zagotta, and D. Veesler. 2017. CryoEM structure of a prokaryotic cyclic nucleotide-gated ion channel. *Proc. Natl. Acad. Sci. USA.* 114:4430–4435. https://doi.org/10.1073/pnas.1700248114

Karpen, J.W., A.L. Zimmerman, L. Stryer, and D.A. Baylor. 1988. Gating kinetics of the cyclic-GMP-activated channel of retinal rods: flash photolysis and voltage-jump studies. *Proc. Natl. Acad. Sci. USA.* 85:1287–1291. https://doi.org/10.1073/pnas.85.4.1287

Kaupp, U.B., and R. Seifert. 2002. Cyclic nucleotide-gated ion channels. *Physiol. Rev.* 82:769–824. https://doi.org/10.1152/physrev.00008.2002

Kaupp, U.B., T. Niidome, T. Tanabe, S. Terada, W. Bönigk, W. Stühmer, N.J. Cook, K. Kangawa, H. Matsuo, T. Hirose, et al. 1989. Primary structure and functional expression from complementary DNA of the rod photoreceptor cyclic GMP-gated channel. *Nature.* 342:762–766. https://doi.org/10.1038/342762a0

Kawate, T., and E. Gouaux. 2006. Fluorescence-detection size-exclusion chromatography for precrystallization screening of integral membrane proteins. *Structure.* 14:673–681. https://doi.org/10.1016/j.str.2006.01.013

Kesters, D., M. Brams, M. Nys, E. Wijckmans, R. Spurny, T. Voets, J. Tytgat, J. Kusch, and C. Ulens. 2015. Structure of the SthK carboxy-terminal region reveals a gating mechanism for cyclic nucleotide-modulated ion channels. *PLoS One.* 10:e0116369. https://doi.org/10.1371/journal.pone.0116369

Kimanius, D., B.O. Forsberg, S.H. Scheres, and E. Lindahl. 2016. Accelerated cryo-EM structure determination with parallelisation using GPUs in RELION-2. *eLife.* 5:5. https://doi.org/10.7554/eLife.18722

Komatsu, H., Y.H. Jin, N. L'Etoile, I. Mori, C.I. Bargmann, N. Akaike, and Y. Ohshima. 1999. Functional reconstitution of a heteromeric cyclic nucleotide-gated channel of *Caenorhabditis elegans* in cultured cells. *Brain Res.* 821:160–168. https://doi.org/10.1016/S0006-8993(99)01111-7

Kowal, J., M. Chami, P. Baumgartner, M. Arheit, P.-L. Chiu, M. Rangl, S. Scheuring, G.F. Schröder, C.M. Nimigean, and H. Stahlberg. 2014. Ligand-induced structural changes in the cyclic nucleotide-modulated potassium channel MloK1. *Nat. Commun.* 5:3106. https://doi.org/10.1038/ncomms4106

Kowal, J., N. Biyani, M. Chami, S. Scherer, A.J. Rzepiela, P. Baumgartner, V. Upadhyay, C.M. Nimigean, and H. Stahlberg. 2018. High-Resolution Cryoelectron Microscopy Structure of the Cyclic Nucleotide-Modulated Potassium Channel MloK1 in a Lipid Bilayer. *Structure.* 26:20–27.e3. https://doi.org/10.1016/j.str.2017.11.012

Kraemer, A., H.R. Rehmann, R.H. Cool, C. Theiss, J. de Rooij, J.L. Bos, and A. Wittinghofer. 2001. Dynamic interaction of cAMP with the Rap guanine-nucleotide exchange factor Epac1. *J. Mol. Biol.* 306:1167–1177. https://doi.org/10.1006/jmbi.2001.4444

Kusch, J., C. Biskup, S. Thon, E. Schulz, V. Nache, T. Zimmer, F. Schwede, and K. Benndorf. 2010. Interdependence of receptor activation and ligand binding in HCN2 pacemaker channels. *Neuron.* 67:75–85. https://doi.org/10.1016/j.neuron.2010.05.022

Lander, G.C., S.M. Stagg, N.R. Voss, A. Cheng, D. Fellmann, J. Pulokas, C. Yoshioka, C. Irving, A. Mulder, P.W. Lau, et al. 2009. Appion: an integrated, database-driven pipeline to facilitate EM image processing. *J. Struct. Biol.* 166:95–102. https://doi.org/10.1016/j.jsb.2009.01.002

Lee, C.H., and R. MacKinnon. 2017. Structures of the Human HCN1 Hyperpolarization-Activated Channel. *Cell.* 168:111–120.e11. https://doi.org/10.1016/j.cell.2016.12.023

LeMasurier, M., L. Heginbotham, and C. Miller. 2001. KcsA: it's a potassium channel. *J. Gen. Physiol.* 118:303–314. https://doi.org/10.1085/jgp.118.3.303

Li, M., X. Zhou, S. Wang, I. Michailidis, Y. Gong, D. Su, H. Li, X. Li, and J. Yang. 2017. Structure of a eukaryotic cyclic-nucleotide-gated channel. *Nature.* 542:60–65. https://doi.org/10.1038/nature20819

Livermore, B.P., and R.C. Johnson. 1974. Lipids of the Spirochaetales: comparison of the lipids of several members of the genera Spirochaeta, Treponema, and Leptospira. *J. Bacteriol.* 120:1268–1273.

Lolicato, M., M. Nardini, S. Gazzarrini, S. Möller, D. Bertinetti, F.W. Herberg, M. Bolognesi, H. Martin, M. Fasolini, J.A. Bertrand, et al. 2011. Tetramerization dynamics of C-terminal domain underlies isoform-specific cAMP gating in hyperpolarization-activated cyclic nucleotide-gated channels. *J. Biol. Chem.* 286:44811–44820. https://doi.org/10.1074/jbc.M111.297606

Ludwig, A., X. Zong, M. Jeglitsch, F. Hofmann, and M. Biel. 1998. A family of hyperpolarization-activated mammalian cation channels. *Nature.* 393:587–591. https://doi.org/10.1038/31255

Nache, V., J. Kusch, V. Hagen, and K. Benndorf. 2006. Gating of cyclic nucleotide-gated (CNGA1) channels by cGMP jumps and depolarizing voltage steps. *Biophys. J.* 90:3146–3154. https://doi.org/10.1529/biophysj.105.078667

Nimigean, C.M. 2006. A radioactive uptake assay to measure ion transport across ion channel-containing liposomes. *Nat. Protoc.* 1:1207–1212. https://doi.org/10.1038/nprot.2006.166

Ohi, M., Y. Li, Y. Cheng, and T. Walz. 2004. Negative Staining and Image Classification - Powerful Tools in Modern Electron Microscopy. *Biol. Proced. Online.* 6:23–34. https://doi.org/10.1251/bpo70

Paoletti, P., E.C. Young, and S.A. Siegelbaum. 1999. C-Linker of cyclic nucleotide-gated channels controls coupling of ligand binding to channel gating. *J. Gen. Physiol.* 113:17–34. https://doi.org/10.1085/jgp.113.1.17

Posson, D.J., R. Rusinova, O.S. Andersen, and C.M. Nimigean. 2018. Stopped-Flow Fluorometric Ion Flux Assay for Ligand-Gated Ion Channel Studies. *Methods Mol. Biol.* 1684:223–235. https://doi.org/10.1007/978-1-4939-7362-0_17

Reddy, S.V., S. Aspana, D.L. Tushar, Ch. Sasikala, and ChV. Ramana. 2013. *Spirochaeta sphaeroplastigenens* sp. nov., a halo-alkaliphilic, obligately anaerobic spirochaete isolated from soda lake Lonar. *Int. J. Syst. Evol. Microbiol.* 63:2223–2228. https://doi.org/10.1099/ijs.0.046292-0

Robinson, R.B., and S.A. Siegelbaum. 2003. Hyperpolarization-activated cation currents: from molecules to physiological function. *Annu. Rev. Physiol.* 65:453–480. https://doi.org/10.1146/annurev.physiol.65.092101.142734

Rusinova, R., D.M. Kim, C.M. Nimigean, and O.S. Andersen. 2014. Regulation of ion channel function by the host lipid bilayer examined by a stopped-flow spectrofluorometric assay. *Biophys. J.* 106:1070–1078. https://doi.org/10.1016/j.bpj.2014.01.027

Santoro, B., D.T. Liu, H. Yao, D. Bartsch, E.R. Kandel, S.A. Siegelbaum, and G.R. Tibbs. 1998. Identification of a gene encoding a hyperpolarization-activated pacemaker channel of brain. *Cell.* 93:717–729. https://doi.org/10.1016/S0092-8674(00)81434-8

Saponaro, A., S.R. Pauleta, F. Cantini, M. Matzapetakis, C. Hammann, C. Donadoni, L. Hu, G. Thiel, L. Banci, B. Santoro, and A. Moroni. 2014. Structural basis for the mutual antagonism of cAMP and TRIP8b in regulating HCN channel function. *Proc. Natl. Acad. Sci. USA.* 111:14577–14582. https://doi.org/10.1073/pnas.1410389111

Scheres, S.H. 2012. RELION: implementation of a Bayesian approach to cryo-EM structure determination. *J. Struct. Biol.* 180:519–530. https://doi.org/10.1016/j.jsb.2012.09.006

Suloway, C., J. Pulokas, D. Fellmann, A. Cheng, F. Guerra, J. Quispe, S. Stagg, C.S. Potter, and B. Carragher. 2005. Automated molecular microscopy: the new Leginon system. *J. Struct. Biol.* 151:41–60. https://doi.org/10.1016/j.jsb.2005.03.010

Tang, C.Y., and D.M. Papazian. 1997. Transfer of voltage independence from a rat olfactory channel to the *Drosophila* ether-à-go-go K+ channel. *J. Gen. Physiol.* 109:301–311. https://doi.org/10.1085/jgp.109.3.301

Thompson, A.N., D.J. Posson, P.V. Parsa, and C.M. Nimigean. 2008. Molecular mechanism of pH sensing in KcsA potassium channels. *Proc. Natl. Acad. Sci. USA.* 105:6900–6905. https://doi.org/10.1073/pnas.0800873105

Varnum, M.D., K.D. Black, and W.N. Zagotta. 1995. Molecular mechanism for ligand discrimination of cyclic nucleotide-gated channels. *Neuron.* 15:619–625. https://doi.org/10.1016/0896-6273(95)90150-7

Voss, N.R., C.K. Yoshioka, M. Radermacher, C.S. Potter, and B. Carragher. 2009. DoG Picker and TiltPicker: software tools to facilitate particle selection in single particle electron microscopy. *J. Struct. Biol.* 166:205–213. https://doi.org/10.1016/j.jsb.2009.01.004

Voss, N.R., D. Lyumkis, A. Cheng, P.W. Lau, A. Mulder, G.C. Lander, E.J. Brignole, D. Fellmann, C. Irving, E.L. Jacovetty, et al. 2010. A toolbox for ab initio 3-D reconstructions in single-particle electron microscopy. *J. Struct. Biol.* 169:389–398. https://doi.org/10.1016/j.jsb.2009.12.005

Wang, Z.X. 1995. An exact mathematical expression for describing competitive binding of two different ligands to a protein molecule. *FEBS Lett.* 360:111–114. https://doi.org/10.1016/0014-5793(95)00062-E

Wilkinson, K.D. 2004. Quantitative analysis of protein-protein interactions. *Methods Mol. Biol.* 261:15–32.

Xu, X., Z.V. Vysotskaya, Q. Liu, and L. Zhou. 2010. Structural basis for the cAMP-dependent gating in the human HCN4 channel. *J. Biol. Chem.* 285:37082–37091. https://doi.org/10.1074/jbc.M110.152033

Yellen, G. 2002. The voltage-gated potassium channels and their relatives. *Nature.* 419:35–42. https://doi.org/10.1038/nature00978

Yu, F.H., and W.A. Catterall. 2003. Overview of the voltage-gated sodium channel family. *Genome Biol.* 4:207. https://doi.org/10.1186/gb-2003-4-3-207

Zagotta, W.N., N.B. Olivier, K.D. Black, E.C. Young, R. Olson, and E. Gouaux. 2003. Structural basis for modulation and agonist specificity of HCN pacemaker channels. *Nature.* 425:200–205. https://doi.org/10.1038/nature01922

Zhou, L., and S.A. Siegelbaum. 2007. Gating of HCN channels by cyclic nucleotides: residue contacts that underlie ligand binding, selectivity, and efficacy. *Structure.* 15:655–670. https://doi.org/10.1016/j.str.2007.04.012